Evolution and Nonreciprocity of Loss-Induced Topological Phase Singularity Pairs

Mengqi Liu,[1,2] Chen Zhao,[2] Yixuan Zeng,[2] Yang Chen,[2] Changying Zhao,[1,*] and Cheng-Wei Qiu[2,†]
[1]*Institute of Engineering Thermophysics, MOE Key Laboratory for Power Machinery and Engineering, School of Mechanical Engineering, Shanghai Jiao Tong University, Shanghai 200240, China*
[2]*Department of Electrical and Computer Engineering, National University of Singapore, Singapore 117583, Singapore*

(Received 7 July 2021; accepted 4 November 2021; published 20 December 2021)

Singular behaviors are increasingly being found in structures supporting bound states in the continuum (BICs), while the nonreciprocity with spectral phase singularity has not been reported. Here, we demonstrate the origin, evolution, and application of topological phase singularity pairs (TPSPs) resulting from BICs in nonreciprocal and non-Hermitian systems. The nonreciprocity contributes to creating accidental BICs asymmetrically, each of which can split into TPSP with topological charges ± 1 in reflection phases by inserting loss. The formation, annihilation, and revival processes of these TPSPs can be selectively controlled via either material or radiative loss. The criteria to predict both number and angular positions of asymmetric BICs are established. Near-complete violation of Kirchhoff's law of thermal radiation has been correspondingly manifested over a wide angular range. The unveiled physics synergizing nonreciprocity and topology will bring new opportunities in multidisciplinary areas like thermal science, magneto-optics, or topological metasurfaces.

DOI: 10.1103/PhysRevLett.127.266101

Singularity is a unique phenomenon where the exact property of the system is ill defined. Various systems exhibit a nontrivial singular nature like black holes, tornados, moire patterns [1], etc. In optics, singularities are seen in phase, polarization, and intensity [2]. For example, phase singularity has been well studied in vortex beams carrying orbital angular momentum [3], where light intensity reaches zero with a singular phase in spatial space. Less attention has been paid to spectral phase singularities [4–8], which also leads to many important applications in high-precise sensing [5,6], unidirectional laser [7], and phase modulation [9], etc.

Recently, singular behaviors have been discovered in systems possessing bound states in the continuum (BICs) [10]. These localized states lie inside the radiation continuum but have infinity lifetimes [11,12], offering a versatile platform to shape light-matter interaction and renovate various technologies [13–16]. Especially, optical singularities with nonzero topological charges play essential roles in such systems. Many efforts have been dedicated to BIC-driven polarization singularities in momentum space [17–20], enabling topologically protected polarization control. The momentum-space polarization responses have been extended to generate singular phases in far-field regions [21], leading to the generation of vortex beams [22] or ultrafast vortex microlasers [13]. However, controlling phase singularities in a spectral space has seldom been discussed. More recently, Sakotic *et al.* [23] studied topological behaviors in planar structures composed of epsilon-near-zero (ENZ) or epsilon-near-pole materials [24,25]. Interestingly, non-Hermitian parameters such as loss or gain can separate BICs into pairs of vortices with nonzero topological charges of opposite signs. Although charge conservation has been studied, the in-depth understanding of evolution trajectory of these singularities remains elusive. Besides, the reported formation of phase singularities is always symmetric, locking up exciting phenomena and applications rooted in asymmetry and restricting dynamic tuning ability. It would be of great value to investigate and engineer the asymmetry in the spectral and angular behaviors, as well as even quantitative features of asymmetric phase singularities and BICs.

On the other hand, the electromagnetic nonreciprocity [26,27] underpins many physical phenomena and extensive technologies. Especially for magneto-optics, one of the main goals in such systems is to realize highly asymmetric wave control, which relies on either high-Q resonances or strong external stimulus [28–31]. Therefore, blending nonreciprocity with high-Q BIC properties should be mutually beneficial, which will certainly spawn a series of new phenomena (e.g., Faraday intensity effect [32]) and facilitate the development of high-efficiency nonreciprocal devices. However, the intriguing physics and consequences of the interplay between them remain unexplored.

Here, by taking advantage of magneto-optical (MO) effects, we explore the formation mechanism of asymmetric topological phase singularity pairs (TPSPs) in reflective systems and unveil their nonreciprocal and topological features. The asymmetric formation, annihilation, and revival processes of loss-induced TPSPs from BICs have been investigated, whose spectral and angular locations can be selectively tuned by material loss and ENZ-layer

thickness. The evolution trajectories of these TPSPs are explicitly dependent on corresponding dispersion relations. Then, the criteria to predict number and asymmetric angles of BICs are also established. The global charge conservation governs the whole evolution, and the sum of topological charges equals zero. Finally, we employ these inspiring behaviors to design nonreciprocal thermal emitters beyond Kirchhoff's law of thermal radiation.

The basic structure consists of a MO ENZ layer, a dielectric interlayer, and a PEC mirror [Fig. 1(a)]. The natural n-InAs material [33], possessing both MO and ENZ responses in the midinfrared region, is employed, which can be replaced by others like InSb [33], Weyl semimetals [34,35], or metamaterials [36,37]. When an external magnetic field $\mathbf{B}$ is applied along the z direction, its permittivity tensor shows as $\bar{\bar{\boldsymbol{\varepsilon}}} = [\varepsilon_{xx}, \varepsilon_{xy}, 0; \varepsilon_{yx}, \varepsilon_{yy}, 0; 0, 0, \varepsilon_{zz}]$, where

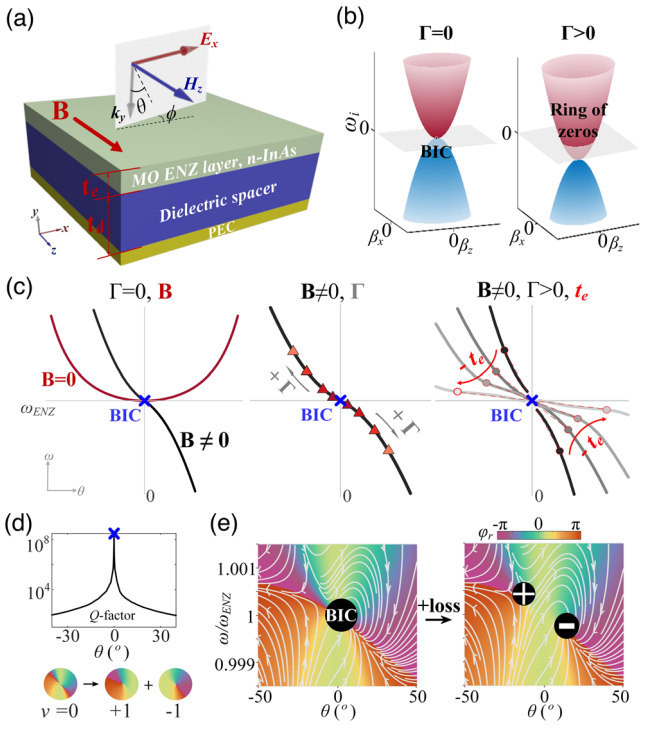

FIG. 1. Generation of TPSPs and nonreciprocal tuning mechanisms. (a) Sketch of the planar structure, illuminated by TM waves (E_x, k_y, H_z). (b) Compared dispersion surfaces of $\omega_i - \beta$ for lossless (left) and lossy (right) cases without $\mathbf{B}$. (c) Shaping the angular and spectral distributions of TPSPs via loss (Γ, middle) and thickness (t_e, right) of the ENZ layer in $\omega - \theta$ spaces. The BICs and TPSPs are denoted by the blue "×" and colored circles (or triangles). The gray (red) arrows show the moving directions when increasing (decreasing) the value of Γ (t_e). The leftmost plot shows dispersion curves with or without $\mathbf{B}$. (d) Q factors for the case at $\mathbf{B} = 0.3$ T and $t_e = 0.5$ μm. The bottom inset shows charge conservation between BIC and TPSP. (e) Phase diagrams φ_r and vector flows of r when $\Gamma = 0$ (left) and $\Gamma = 5 \times 10^{10}$ rad/s (right). Results in (b)–(e) are analyzed without the dielectric spacer.

$\varepsilon_{xx} = \varepsilon_{yy} = \varepsilon_\infty - \omega_p^2(\omega + i\Gamma)/\{\omega[(\omega + i\Gamma)^2 - \omega_c^2]\}$, $\varepsilon_{xy} = -\varepsilon_{yx} = i\omega_p^2\omega_c/\{\omega[(\omega + i\Gamma)^2 - \omega_c^2]\}$ and $\varepsilon_{zz} = \varepsilon_\infty - \omega_p^2/[\omega(\omega + i\Gamma)]$. In addition, $\varepsilon_\infty = 12.37$ is the high-frequency permittivity. The $\omega_p = \sqrt{n_e e^2/(m^*\varepsilon_0)}$ and $\omega_c = e\mathbf{B}/m^*$ are plasma and cyclotron frequencies ($m^* = 0.033m_e$,m_e is the electron mass). The reciprocity could be broken under TM polarization when $\mathbf{B} \neq 0$. Importantly, $\Gamma = e/(m^*\mu)$ is related to optical loss, which can be controlled by electron mobility μ in experiments [38,39]. Here, we assume a doping concentration $n_e = 7.8 \times 10^{17}$ cm^{-3} [31]. Generally, the value of $\eta = |\varepsilon_{xy}|/|\varepsilon_{xx}|$ measures MO strength, thereby one can expect $\eta \to \infty$ since there is $\varepsilon_{xx} \to 0$ at the ENZ frequency ω_{ENZ}. Without losing generality, we use the normalized frequency $\omega/\omega_{\mathrm{ENZ}}$ in the following, despite slight changes of ω_{ENZ} with the $\mathbf{B}$ (Fig. S1) [40].

To show the origin of TPSPs, we begin with a simple case without the dielectric spacer. Such a single-layer structure supports radiative Berreman modes governed by [40]

$$\tan(\kappa_e t_e) = \frac{\varepsilon_{xx}\kappa_e \cdot \gamma}{\varepsilon_{xx}k^2 - \beta^2 + i\varepsilon_{xy}\beta \cdot \gamma}, \tag{1}$$

where $\kappa_e = \sqrt{k^2(\varepsilon_{xx} + \varepsilon_{xy}^2/\varepsilon_{xx}) - \beta^2}$ and $\gamma = \sqrt{\beta^2 - k^2}$ ($k = \omega/c$, c is the light speed in vacuum). Within the light cone, $\beta = [\beta_x, \beta_z] = [k\sin\theta\cos\phi, k\sin\theta\sin\phi]$ is the propagation constant, where θ and ϕ are incident angles respect to the y and x directions [Fig. 1(a)]. The eigenmodes of Eq. (1) can be analyzed in complex frequency ($\bar{\omega} = \omega + i\omega_i$) [60]. We first focus on reciprocal cases to build connections between BICs and TPSPs. In the lossless limit, the zero and pole of dispersion in $\omega_i - \beta$ space touch on the real-frequency axis ($\omega_i = 0$), forming a symmetry-protected BIC [23,40] at $(\omega_{ENZ}, \beta = 0)$ [Figs. 1(b)–1(c), left]. When the loss is introduced ($\Gamma > 0$), the dispersion surface will translate down along the imaginary frequency axis, thus yielding a ring of real-frequency zeros [Fig. 1(b), right]. For a 2D space like $\bar{\omega} - \beta_x(\phi = 0)$ plane mainly discussed here, one can obtain two real-frequency zero points. Such zero points in dispersion predict reflection zeros ($|r|^2 = 0$) [25,45] associated with singular phases in one-port systems, where the reflection coefficients r can be calculated by scattering matrix $\mathrm{S} = [r]$ ($r = |r|e^{i\varphi_r}$, φ_r is the reflection phase).

However, the loss-induced singular phases behave diversely in the presence of $\mathbf{B}$ owing to asymmetric dispersion in Fig. 1(c). The BIC still locates at $\theta = 0°$ having an infinite Q factor [Fig. 1(d), top] and a diverging phase point [Fig. 1(e), left]. But the two phase singularities are asymmetrically rotated around the central BIC in the presence of loss. By tracing an anticlockwise closed loop C around a singularity in $\omega - \theta$ space [Fig. 1(e), right], a total accumulated phase of $\pm 2\pi$ can be obtained, indicating integer topological charges $\nu = (1/2\pi)\oint_C d\varphi_r = \pm 1$ [23].

The bottom inset in Fig. 1(d) illustrates the charge conversation between BIC ($\nu = 0$) and TPSPs. Here, two loss tuning methods are proposed to precisely control the distributions of these asymmetric TPSPs. One feasible way is to modify material loss in the ENZ layer, where the angular and spectral distance of TPSP will be lengthened along the initial dispersion for a large Γ [Fig. 1(c), middle]. Besides, reducing the upper layer thickness helps to strengthen the radiative loss, where the TPSPs keep pace with rotated dispersion curves around the BIC [Fig. 1(c)), right]. The detailed evolution of TPSP from 0° BIC is given in the Supplemental Material, Note 3 [40]. Notably, two opposite phase singularities from the same BIC will be present until meeting another opposite one.

Then, we activate the dielectric spacer and set its permittivity as $\varepsilon_d = 2$ unless otherwise stated. The dielectric spacer supports Fabry-Perot (FP) resonances under certain conditions, overlapping with Berreman modes off $\theta = 0°$ thus creating accidental BICs [25,45]. For nonreciprocal cases, how those accidental BICs are formed and located is not known yet. The governed dispersion of guided modes changes to

$$\tan(\kappa_e t_e) = \frac{\varepsilon_{xy}\beta - i[\gamma(\varepsilon_{xx}^2 + \varepsilon_{xy}^2) + \varepsilon_{xx}\kappa_e \cdot \mathbf{M}]}{-\varepsilon_{xy}\beta \cdot \mathbf{M} + i[\gamma(\varepsilon_{xx}^2 + \varepsilon_{xy}^2) \cdot \mathbf{M} - \varepsilon_{xx}\kappa_e]}. \quad (2)$$

We introduce a parameter $\mathbf{M}$ that evaluates the roles of both dielectric layer and MO effect by

$$\mathbf{M} = -i\frac{\varepsilon_{xy}\beta}{\varepsilon_{xx}\kappa_e} - \frac{\varepsilon_{xx}^2 + \varepsilon_{xy}^2}{\varepsilon_{xx}\kappa_e}\frac{\kappa_d}{\varepsilon_d}\tan(\kappa_d t_d), \quad (3)$$

where $\kappa_d = \sqrt{\varepsilon_d k^2 - \beta^2}$. We find that the roots of $\mathbf{M}$ at ω_{ENZ} correspond to the poles of Eq. (2) for $\varepsilon_{xx} \to 0$. The overlapping of roots and poles predict the generation of BICs [61]. We assume $t_d = (L^n/2)(\lambda_{\mathrm{ENZ}}/\sqrt{\varepsilon_d})$ ($L^n \in \mathbf{R}^*$, $\lambda_{\mathrm{ENZ}} = 2\pi c/\omega_{\mathrm{ENZ}}$), then the solutions of $\mathbf{M} = 0$ lead to [40]

$$L^n(\theta) = \frac{\frac{1}{\pi}\cdot \arctan\left(\frac{\varepsilon_d}{i\varepsilon_{xy}}\cdot\frac{\sin\theta}{\sqrt{\varepsilon_d - \sin^2\theta}}\right) + n}{\sqrt{(\varepsilon_d - \sin^2\theta)/\varepsilon_d}}, \qquad n = 0, 1, 2\ldots \quad (4)$$

The MO effects and FP resonances are encoded in Eq. (4) evaluated at angles where BICs occur. It is obvious that $L^n(\theta, n) \neq L^n(-\theta, n)$, indicating a series of asymmetric BICs and TPSPs. Without $\mathbf{B}$, the Eq. (4) reduces to $L^n = [(2n+1)/2]\sqrt{\varepsilon_d/(\varepsilon_d - \sin^2\theta)}$, agreeing with the general FP conditions of $t_d = [(2n+1)/4](\lambda_{\mathrm{ENZ}}/\sqrt{\varepsilon_d - \sin^2\theta})$ [23,40].

Next, we unveil the diverse evolution behaviors of several TPSPs from different BICs. Figure 2(a) shows the trajectory of TPSPs changing with the material loss (triangles) and ENZ-layer thickness (circles) at $\mathbf{B} = 0.3$ T and $L^n = 1.75$. There are three asymmetric BICs

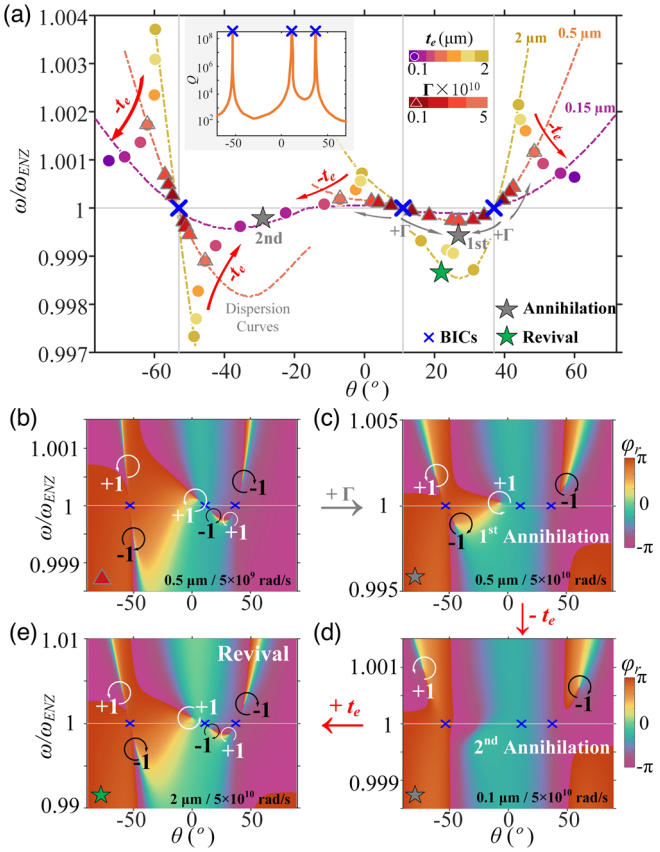

FIG. 2. Evolution of asymmetric TPSPs when changing the ENZ layer's thickness and loss. (a) Trajectories of TPSPs from three BICs (blue "×"). Three dashed lines are dispersion curves for different t_e: 0.15 μm (purple), 0.5 μm (orange), and 2 μm (yellow). The gray (red) arrows show the moving directions of TPSPs marked in colored triangles (circles) when increasing (decreasing) the value of Γ (t_e), at a fixed $t_e = 0.5$ μm ($\Gamma = 5 \times 10^{10}$ rad/s). The inset gives Q factors at $t_e = 0.5$ μm. (b) A typical case supporting three coupled TPSPs at $t_e = 0.5$ μm and $\Gamma = 5 \times 10^9$ rad/s. Two sequential annihilation processes when (c) increasing the Γ to 5×10^{10} rad/s and (d) further reducing the thickness to $t_e = 0.1$ μm. (e) Charges revival at a large thickness $t_e = 2$ μm. All data are analyzed at $\mathbf{B} = 0.3$ T and $L^n = 1.75$.

(blue "×") located at −53°, 11° and 37° (see infinite Q factors in the inset). For a given $t_e = 0.5$ μm, initially, three coupled TPSPs emerge at a small loss near the BICs [Fig. 2(b)]. When the Γ is increasingly added, the TPSPs from −53°-BIC keep walking along the left branch of dispersion (orange line). Differently, the two right neighboring phase singularities will be gradually closer to each other until encountering and mutually annihilating (1st gray pentagram) for a larger loss [Fig. 2(c)]. At a fixed $\Gamma = 5 \times 10^{10}$ rad/s, further decreasing t_e helps to modify dispersion curves and evolution directions of TPSPs (red arrows), leading to the 2nd annihilation of the other two adjacent singularities [Fig. 2(d)]. The annihilation order is determined by both dispersion profiles and Q factor of TPSPs [40]. In contrast, the vanished charges can also be

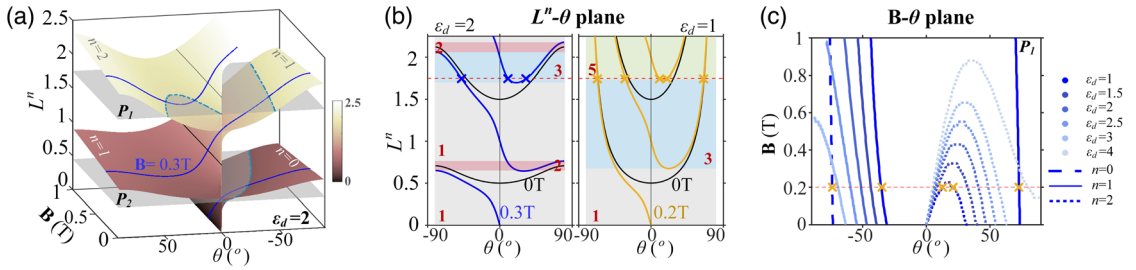

FIG. 3. Number and position selection criteria for asymmetric BICs. (a) Blooming flower patterns for predicting the angles θ and number of BICs when $\varepsilon_d = 2$. (b) Projection of $L^n - \theta$ plane for typical cases: $\varepsilon_d = 2$, $\mathbf{B} = 0.3$ T (left) and $\varepsilon_d = 1$, $\mathbf{B} = 0.2$ T (right). The number of BICs is marked in each shaded region. (c) Influence of ε_d in angular distributions of BICs in $\mathbf{B} - \theta$ space. The red dashed lines in (b)–(c) denote a typical case at $L^n = 1.75$, where the BICs are marked with "×."

revived using a thick ENZ layer [Fig. 2(e), green pentagram] [62]. The formation and annihilation of two TPSPs are symmetric in the absence of $\mathbf{B}$.

As revealed above, the BICs give rise to loss-induced TPSPs and work as their starting points in reflection phase spectra. According to Eq. (4), the locations and total numbers of BICs can be explicitly determined by $t_d \sim L^n$. The magnitude of $\mathbf{B}$, dielectric permittivity ε_d and integer order n play critical roles in shaping the profile of $L^n(\theta, \mathbf{B}, n, \varepsilon_d)$. For a given dielectric spacer ($\varepsilon_d = 2$), the distribution of BICs shows a flower-like pattern [Fig. 3(a)]. The full blue lines in Fig. 3(a) denote angular positions of BICs at $\mathbf{B} = 0.3$ T projected in $L^n - \theta$ space [Fig. 3(b), left], which are gradually asymptotic to the symmetric results (black lines) at large angles. The amount of BICs for different L^n can be determined by boundary conditions and is marked in individual regions. Table S1 in the Supplemental Material gives specific criteria to predict the number of BICs and corresponding located angular range. There are two critical boundaries: one is $L^n(\pm 90°)$ working as light lines where BICs will disappear for $|\theta| > 90°$, and the other is $\min(L^n)$ regarded as "birth lines" for creating new BICs [40]. For example, in Fig. 3(b) (left), the case of $L^n = 1.75$ (red dashed line) lies within the range of $\min(L^2) < L^n < L^1(-90°)$, creating three BICs (blue "×") in Fig. 2. On the other hand, the permittivity of the dielectric spacer is also essential in shaping flowerlike patterns. The intersection lines of the gray planes ($\boldsymbol{P}_{1,2}$) denote the BICs in $\mathbf{B} - \theta$ space for a given $t_d(L^n)$. Movie S1 in the Supplemental Material [40] shows the dynamic process of BICs' locations by increasing ε_d, where the intersecting lines for different n gradually shift to $L^n(\pm 90°)$. In Fig. 3(c), for example, five asymmetric BICs appear when choosing an airlike spacer (Fig. S6 [40]). Notably, for a small L^n like case P_2, there is only one off-0° BIC whose position can be tuned via either $\mathbf{B}$ or ε_d, different from the symmetry-protected BIC pinned at $\theta = 0°$ subject to reciprocity. The role of substrate in redistributing BICs and TPSPs is discussed in the Supplemental Material [40].

Last but not least, we employ TPSPs to engineer nonreciprocal thermal radiation since phase singularities also manifest as topologically protected perfect absorption [63]. Nonreciprocal thermal radiation is an emerging state-of-art area to break Kirchhoff's law of thermal radiation. This classical law indicates the equality of emissivity $e(\omega, \theta)$ and absorptivity $\alpha(\omega, \theta)$ with an intrinsic loss [64,65], which is not required by thermodynamic laws but rather originates from Lorentz reciprocity [66,67]. So, it can be violated by designing nonreciprocal thermal emitters composed of, i.e., MO materials, providing new possibilities to shape emission and absorption separately and open up exciting frontiers for next-generation energy devices like time-asymmetric photovoltaics [68], thermophotovoltaic [69], and radiative cooling [70]. Nevertheless, few thermal emitters can completely violate Kirchhoff's law ($|e - \alpha| \to 1$) [31,41,50–54,71,72]. Fan's group has done several seminal works [31,41,50,71], but almost all of them depend on asymmetric coupling with gratings. Then, the large nonreciprocity can only be realized by peak shifts [Fig. 4(a), middle], relying on either high-Q resonances or a large $\mathbf{B}$. Besides, coupling conditions only ensure perfect emission peaks at specific angles, i.e., >60°. Therefore, to flexibly engineer nonreciprocal thermal radiation is still an open challenge.

The asymmetric TPSPs offer great possibilities in nonreciprocal radiation control, where the absorptivity can be spectrally suppressed with a perfect emissivity peak, as exampled in Fig. 4(a). We adopt a fixed $\Gamma = 1.55 \times 10^{11}$ rad/s [31,41] for better comparison. Figure 4(b) gives the results of $\alpha = 1 - R_\theta$ and $e = 1 - R_{-\theta}$ at $\mathbf{B} = 0.3$ T, supporting four phase singularities (white circles). The emission and absorption spectra are no longer symmetric, and large nonreciprocity has been realized with $|\alpha - e| \approx 1$ over a wide angular range. An asymmetric angular pattern at singular ω_A is exampled in Fig. 4(b) (right). Further, we show topological robustness of TPSPs-induced nonreciprocal radiation. The structures containing two singularities from an off-0° BIC are considered (Fig. S8 [40]). In Figs. 4(c)–4(d), the working angle of nonreciprocal absorption can be continuously tuned via the geometric parameter at a small $\mathbf{B} = 0.1$ T, as long as the topological feature is not changed. Besides, our asymmetric TPSPs-based

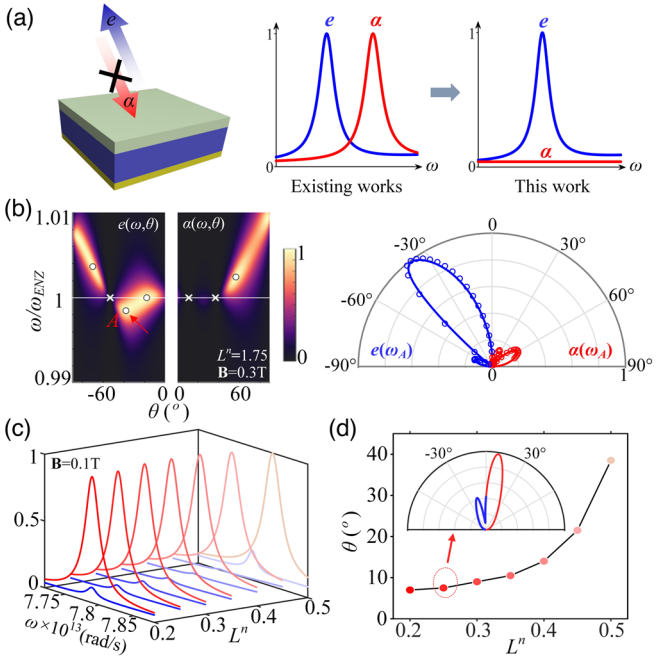

FIG. 4. Nonreciprocal thermal radiation based on asymmetric TPSPs. (a) Compared principles to realize perfect nonreciprocal thermal emitters. (b) Asymmetric emission and absorption spectra with two TPSPs (white circles) at $L^n = 1.75$, $t_e = 0.5$ μm, and $\mathbf{B} = 0.3$ T, along with a radiation pattern at ω_A (right). The full lines and dots are results obtained by scattering matrix and full-wave simulation. (c) Evolution of emission and absorption spectra via continuously tuning of L^n at $\mathbf{B} = 0.1$ T and $t_e = 5$ μm. (d) The corresponding working angles for cases in (c). The inset shows a typical angular diagram at $L^n = 0.25$.

nonreciprocal thermal emitters can also be achieved using Weyl semimetals with intrinsic magnetism [40].

In conclusion, we have demonstrated the deterministic generation, dispersion-guided evolution of loss-induced TPSPs with ± 1 topological charges in nonreciprocal systems. The annihilation and revival of these TPSPs can be asymmetrically engineered by modifying the system loss. We propose explicit criteria to evaluate and predict the existence and number of asymmetric BICs and TPSPs determined by geometric and material parameters. We apply our discoveries specifically in the application of nonreciprocal thermal emitters. The combined merits of nonreciprocity and topology shed new light on high-efficiency devices, like unidirectional waveguides, nonreciprocal light-harvesting devices, topological metasurfaces, etc.

C. Y. Z. acknowledges the National Natural Science Foundation of China (No. 52120105009, No. 51636004, and No. 51906144) and the Shanghai Key Fundamental Research Grant (No. 20JC1414800). C.-W. Q. acknowledges the financial support of the Ministry of Education, Republic of Singapore (Grant No. R-263-000-E19-114). M. Q. L. acknowledges the support from SJTU-NUS Joint PhD Project.

*changying.zhao@sjtu.edu.cn
†chengwei.qiu@nus.edu.sg

[1] J. R. Leonard, L. Hu, A. A. High, A. T. Hammack, C. Wu, L. V. Butov, K. L. Campman, and A. C. Gossard, Moiré pattern of interference dislocations in condensate of indirect excitons, Nat. Commun. **12**, 1175 (2021).
[2] G. J. Gbur, *Singular Optics* (CRC Press, Boca Raton, 2016).
[3] Y. Shen, X. Wang, Z. Xie, C. Min, X. Fu, Q. Liu, M. Gong, and X. Yuan, Optical vortices 30 years on: OAM manipulation from topological charge to multiple singularities, Light **8**, 90 (2019).
[4] Z. Han, S. Ohno, and H. Minamide, Spectral phase singularity in a transmission-type double-layer metamaterial, Optica **7**, 1721 (2020).
[5] V. G. Kravets, F. Schedin, R. Jalil, L. Britnell, R. V. Gorbachev, D. Ansell, B. Thackray, K. S. Novoselov, A. K. Geim, A. V. Kabashin, and A. N. Grigorenko, Singular phase nano-optics in plasmonic metamaterials for label-free single-molecule detection, Nat. Mater. **12**, 304 (2013).
[6] K. V. Sreekanth, S. Sreejith, S. Han, A. Mishra, X. Chen, H. Sun, C. T. Lim, and R. Singh, Biosensing with the singular phase of an ultrathin metal-dielectric nanophotonic cavity, Nat. Commun. **9**, 369 (2018).
[7] H. Ramezani, H. K. Li, Y. Wang, and X. Zhang, Unidirectional Spectral Singularities, Phys. Rev. Lett. **113**, 263905 (2014).
[8] Y. Li and C. Argyropoulos, Exceptional points and spectral singularities in active epsilon-near-zero plasmonic waveguides, Phys. Rev. B **99**, 075413 (2019).
[9] H. T. Chen, W. J. Padilla, M. J. Cich, A. K. Azad, R. D. Averitt, and A. J. Taylor, A metamaterial solid-state terahertz phase modulator, Nat. Photonics **3**, 148 (2009).
[10] W. Liu, W. Liu, L. Shi, and Y. Kivshar, Topological polarization singularities in metaphotonics, Nanophotonics **10**, 1469 (2021).
[11] C. W. Hsu, B. Zhen, A. D. Stone, J. D. Joannopoulos, and M. Soljacic, Bound states in the continuum, Nat. Rev. Mater. **1**, 16048 (2016).
[12] K. Koshelev, S. Lepeshov, M. Liu, A. Bogdanov, and Y. Kivshar, Asymmetric Metasurfaces with High-Q Resonances Governed by Bound States in the Continuum, Phys. Rev. Lett. **121**, 193903 (2018).
[13] C. Huang, C. Zhang, S. Xiao, Y. Wang, Y. Fan, Y. Liu, N. Zhang, G. Qu, H. Ji, J. Han, L. Ge, Y. Kivshar, and Q. Song, Ultrafast control of vortex microlasers, Science **367**, 1018 (2020).
[14] A. Kodigala, T. Lepetit, Q. Gu, B. Bahari, Y. Fainman, and B. Kanté, Lasing action from photonic bound states in continuum, Nature (London) **541**, 196 (2017).
[15] S. I. Azzam and A. V. Kildishev, Photonic bound states in the continuum: From basics to applications, Adv. Opt. Mater. **9**, 2001469 (2021).
[16] X. Yin, J. Jin, M. Soljačić, C. Peng, and B. Zhen, Observation of topologically enabled unidirectional guided resonances, Nature (London) **580**, 467 (2020).
[17] H. M. Doeleman, F. Monticone, W. Den Hollander, A. Alù, and A. F. Koenderink, Experimental observation of a polarization vortex at an optical bound state in the continuum, Nat. Photonics **12**, 397 (2018).

[18] B. Zhen, C. W. Hsu, L. Lu, A. D. Stone, and M. Soljačić, Topological Nature of Optical Bound States in the Continuum, Phys. Rev. Lett. **113**, 257401 (2014).
[19] Y. Zhang, A. Chen, W. Liu, C. W. Hsu, B. Wang, and F. Guan, Observation of Polarization Vortices in Momentum Space, Phys. Rev. Lett. **120**, 186103 (2018).
[20] W. Liu, B. Wang, Y. Zhang, J. Wang, M. Zhao, F. Guan, X. Liu, L. Shi, and J. Zi, Circularly Polarized States Spawning from Bound States in the Continuum, Phys. Rev. Lett. **123**, 116104 (2019).
[21] X. Liu, S. Xia, E. Jajtić, D. Song, D. Li, L. Tang, D. Leykam, J. Xu, H. Buljan, and Z. Chen, Universal momentum-to-real-space mapping of topological singularities, Nat. Commun. **11**, 1 (2020).
[22] B. Wang, W. Liu, M. Zhao, J. Wang, Y. Zhang, A. Chen, F. Guan, X. Liu, L. Shi, and J. Zi, Generating optical vortex beams by momentum-space polarization vortices centred at bound states in the continuum, Nat. Photonics **14**, 623 (2020).
[23] Z. Sakotic, A. Krasnok, A. Alú, and N. Jankovic, Topological scattering singularities and embedded eigenstates for polarization control and sensing applications, Photonics Res. **9**, 1310 (2021).
[24] F. Monticone, H. M. Doeleman, W. Den Hollander, A. F. Koenderink, and A. Alù, Trapping light in plain sight: Embedded photonic eigenstates in zero-index metamaterials, Laser Photonics Rev. **12**, 1700220 (2018).
[25] Z. Sakotic, A. Krasnok, N. Cselyuszka, N. Jankovic, and A. Alù, Berreman Embedded Eigenstates for Narrow-Band Absorption and Thermal Emission, Phys. Rev. Applied **13**, 064073 (2020).
[26] V. S. Asadchy, M. S. Mirmoosa, A. Diaz-Rubio, S. Fan, and S. A. Tretyakov, Tutorial on electromagnetic nonreciprocity and its origins, Proc. IEEE **108**, 1684 (2020).
[27] C. Caloz, A. Alù, S. Tretyakov, D. Sounas, K. Achouri, and Z.-L. Deck-Léger, Electromagnetic Nonreciprocity, Phys. Rev. Applied **10**, 047001 (2018).
[28] G. Armelles, A. Cebollada, A. García-Martín, and M. U. González, Magnetoplasmonics: Combining magnetic and plasmonic functionalities, Adv. Opt. Mater. **1**, 10 (2013).
[29] H. Lu, Z. Yue, Y. Li, Y. Zhang, M. Zhang, W. Zeng, X. Gan, D. Mao, F. Xiao, T. Mei, W. Zhao, X. Wang, M. Gu, and J. Zhao, Magnetic plasmon resonances in nanostructured topological insulators for strongly enhanced light–MoS_2 interactions, Light **9**, 191 (2020).
[30] M. G. Barsukova, A. S. Shorokhov, A. I. Musorin, D. N. Neshev, Y. S. Kivshar, and A. A. Fedyanin, Magneto-optical response enhanced by Mie resonances in nanoantennas, ACS Photonics **4**, 2390 (2017).
[31] L. Zhu and S. Fan, Near-complete violation of detailed balance in thermal radiation, Phys. Rev. B **90**, 220301 (2014).
[32] D. O. Ignatyeva and V. I. Belotelov, Bound states in the continuum enable modulation of light intensity in the Faraday configuration, Opt. Lett. **45**, 6422 (2020).
[33] A. Scheer, H. Kruppke, and R. Heib, *Semiconductors: Data Handbook*, 3rd ed. (Springer-Verlag, Berlin Heidelberg GmbH, 2001).
[34] B. Q. Lv, H. M. Weng, B. B. Fu, X. P. Wang, H. Miao, J. Ma, P. Richard, X. C. Huang, L. X. Zhao, G. F. Chen, Z. Fang, X. Dai, T. Qian, and H. Ding, Experimental Discovery of Weyl Semimetal TaAs, Phys. Rev. X **5**, 031013 (2015).
[35] D. F. Liu, A. J. Liang, E. K. Liu, Q. N. Xu, Y. W. Li, C. Chen, D. Pei, W. J. Shi, S. K. Mo, P. Dudin, T. Kim, C. Cacho, G. Li, Y. Sun, L. X. Yang, Z. K. Liu, S. S. P. Parkin, C. Felser, and Y. L. Chen, Magnetic Weyl semimetal phase in a Kagomé crystal, Science **365**, 1282 (2019).
[36] I. A. Kolmychek, A. R. Pomozov, A. P. Leontiev, K. S. Napolskii, and T. V. Murzina, Magneto-optical effects in hyperbolic metamaterials, Opt. Lett. **43**, 3917 (2018).
[37] P. Huo, S. Zhang, Y. Liang, Y. Lu, and T. Xu, Hyperbolic metamaterials and metasurfaces: Fundamentals and applications, Adv. Opt. Mater. **7**, 1801616 (2019).
[38] D. Li and C. Z. Ning, All-semiconductor active plasmonic system in mid-infrared wavelengths, Opt. Express **19**, 14594 (2011).
[39] M. E. A. Panah, L. Han, K. Norrman, N. Pryds, A. Nadtochiy, A. E. Zhukov, A. V. Lavrinenko, and E. S. Semenova, Mid-IR optical properties of silicon doped InP, Opt. Mater. Express **7**, 2260 (2017).
[40] See Supplemental Material at http://link.aps.org/supplemental/10.1103/PhysRevLett.127.266101 for Notes: 1. Epsilon-near-zero properties of *n*-InAs materials; 2. Dispersion derivation of multilayer MO structures; 3. Nonreciprocal evolution of topological phase singularity pairs; 4. Basic rules for predicting number and position of BICs in nonreciprocal systems; 5. Manipulation of nonreciprocal thermal radiation; 6. The role of mirrorlike semispace substrate; 7. Considerations for experimental realization, which includes Refs. [41–59].
[41] B. Zhao, Y. Shi, J. Wang, Z. Zhao, N. Zhao, and S. Fan, Near-complete violation of Kirchhoff's law of thermal radiation with a 0.3 T magnetic field, Opt. Lett. **44**, 4203 (2019).
[42] Y. M. Strelniker and D. J. Bergman, Itinerant versus localized plasmons in an assembly of metal-dielectric parallel flat slabs in the presence of a perpendicular magnetic field: Faraday and magneto-optical Kerr effects, Phys. Rev. B **103**, 205302 (2021).
[43] A. D. Bresler, On the TE_{n0} modes of a ferrite slab loaded rectangular waveguide and the associated thermodynamic paradox, IRE Trans. Microwave Theory Tech. **8**, 81 (1960).
[44] L. D. S. de Alcantara, Optical propagation in magneto-optical materials, in *Electromagnetic Materials and Devices* (IntechOpen, London, 2018), pp. 137–144.
[45] R. Duggan, Y. Ra'Di, and A. Alù, Temporally and spatially coherent emission from thermal embedded eigenstates, ACS Photonics **6**, 2949 (2019).
[46] S. Y. Xu, I. Belopolski, N. Alidoust, M. Neupane, G. Bian, C. Zhang, R. Sankar, G. Chang, Z. Yuan, C. C. Lee, S. M. Huang, H. Zheng, J. Ma, D. S. Sanchez, B. K. Wang, A. Bansil, F. Chou, P. P. Shibayev, H. Lin, S. Jia, and M. Z. Hasan, Discovery of a Weyl fermion semimetal and topological Fermi arcs, Science. **349**, 613 (2015).
[47] Q. Wang, Y. Xu, R. Lou, Z. Liu, M. Li, Y. Huang, D. Shen, H. Weng, S. Wang, and H. Lei, Large intrinsic anomalous Hall effect in half-metallic ferromagnet $Co_3Sn_2S_2$ with magnetic Weyl fermions, Nat. Commun. **9**, 3681 (2018).
[48] N. J. Ghimire, A. S. Botana, J. S. Jiang, J. Zhang, Y. S. Chen, and J. F. Mitchell, Large anomalous Hall effect in the

chiral-lattice antiferromagnet $CoNb_3S_6$, Nat. Commun. **9**, 3280 (2018).
[49] K. Halterman, M. Alidoust, and A. Zyuzin, Epsilon-near-zero response and tunable perfect absorption in Weyl semimetals, Phys. Rev. B **98**, 085109 (2018).
[50] B. Zhao, C. Guo, C. A. C. Garcia, P. Narang, and S. Fan, Axion-field-enabled nonreciprocal thermal radiation in Weyl semimetals, Nano Lett. **20**, 1923 (2020).
[51] Y. Tsurimaki, X. Qian, S. Pajovic, F. Han, M. Li, and G. Chen, Large nonreciprocal absorption and emission of radiation in type-I Weyl semimetals with time reversal symmetry breaking, Phys. Rev. B **101**, 165426 (2020).
[52] X. Wu, Z. Chen, and F. Wu, Strong nonreciprocal radiation in a InAs film by critical coupling with a dielectric grating, ES Energy Environ. **13**, 8 (2021).
[53] X. Wu, R. Liu, H. Yu, and B. Wu, Strong nonreciprocal radiation in magnetophotonic crystals, J. Quant. Spectrosc. Radiat. Transfer **272**, 107794 (2021).
[54] J. Wu, F. Wu, and X. Wu, Strong dual-band nonreciprocal radiation based on a four-part periodic metal grating, Opt. Mater. **120**, 111476 (2021).
[55] J. Chochol, K. Postava, M. Čada, M. Vanwolleghem, M. Mičica, L. Halagačka, J. F. Lampin, and J. Pištora, Plasmonic behavior of III-V semiconductors in far-infrared and terahertz range, J. Eur. Opt. Soc. **13**, 13 (2017).
[56] M. Liu and C. Zhao, Ultranarrow and wavelength-scalable thermal emitters driven by high-order antiferromagnetic resonances in dielectric nanogratings, ACS Appl. Mater. Interfaces **13**, 25306 (2021).
[57] Z. Che, Y. Zhang, W. Liu, M. Zhao, J. Wang, W. Zhang, F. Guan, X. Liu, W. Liu, L. Shi, and J. Zi, Polarization Singularities of Photonic Quasicrystals in Momentum Space, Phys. Rev. Lett. **127**, 043901 (2021).
[58] B. Zhen, C. W. Hsu, Y. Igarashi, L. Lu, I. Kaminer, A. Pick, S. L. Chua, J. D. Joannopoulos, and M. Soljačić, Spawning rings of exceptional points out of Dirac cones, Nature (London) **525**, 354 (2015).
[59] G. Ermolaev, K. Voronin, D. G. Baranov, V. Kravets, G. Tselikov, Y. Stebunov, D. Yakubovsky, S. Novikov, A. Vyshnevyy, A. Mazitov, I. Kruglov, S. Zhukov, R. Romanov, A. M. Markeev, A. Arsenin, K. S. Novoselov, A. N. Grigorenko, and V. Volkov, Topological phase singularities in atomically thin high-refractive-index materials, arXiv:2106.12390.
[60] A. Archambault, T. V. Teperik, F. Marquier, and J. J. Greffet, Surface plasmon Fourier optics, Phys. Rev. B **79**, 195414 (2009).
[61] A. Krasnok, D. Baranov, H. Li, M.-A. Miri, F. Monticone, and A. Alú, Anomalies in light scattering, Adv. Opt. Photonics **11**, 892 (2019).
[62] From another point of view, the revival process is to find a balance between material loss and radiative loss of the system to meet critical coupling conditions ($|r|^2 = 0$) in angular reflection spectra.
[63] A. Berkhout and A. F. Koenderink, Perfect absorption and phase singularities in plasmon antenna array etalons, ACS Photonics **6**, 2917 (2019).
[64] G. Kirchhoff, I. On the relation between the radiating and absorbing powers of different bodies for light and heat, London, Edinburgh, Dublin Philos. Mag. J. Sci. **20**, 1 (1860).
[65] Z. M. Zhang, X. Wu, and C. Fu, Validity of Kirchhoff's law for semitransparent films made of anisotropic materials, J. Quant. Spectrosc. Radiat. Transfer **245**, 106904 (2020).
[66] M. Krüger, G. Bimonte, T. Emig, and M. Kardar, Trace formulas for nonequilibrium Casimir interactions, heat radiation, and heat transfer for arbitrary objects, Phys. Rev. B **86**, 115423 (2012).
[67] W. C. Snyder, Z. Wan, and X. Li, Thermodynamic constraints on reflectance reciprocity and Kirchhoff's law, Appl. Opt. **37**, 3464 (1998).
[68] M. A. Green, Time-asymmetric photovoltaics, Nano Lett. **12**, 5985 (2012).
[69] T. Burger, C. Sempere, B. Roy-Layinde, and A. Lenert, Present efficiencies and future opportunities in thermophotovoltaics, Joule **4**, 1660 (2020).
[70] M. Wei, W. Wu, D. Li, H. Xu, Y. Lu, and W. Song, Universal strategy for all-weather and all-terrain radiative cooling with non-reciprocal mid-infrared windows, Solar Energy **207**, 471 (2020).
[71] D. A. B. Miller, L. Zhu, and S. Fan, Universal modal radiation laws for all thermal emitters, Proc. Natl. Acad. Sci. U.S.A. **114**, 4336 (2017).
[72] Y. Hadad, J. C. Soric, and A. Alù, Breaking temporal symmetries for emission and absorption, Proc. Natl. Acad. Sci. U.S.A. **113**, 3471 (2016).